J Solid State Electrochem (2015) 19:1783–1791
DOI 10.1007/s10008-015-2789-8

ORIGINAL PAPER

Mesoporous activated carbon spheres derived from resorcinol-formaldehyde resin with high performance for supercapacitors

Yiliang Wang · Binbin Chang · Daxiang Guan · Xiaoping Dong

Received: 6 January 2015 / Revised: 10 February 2015 / Accepted: 12 February 2015 / Published online: 18 March 2015

Abstract Porous electrode materials with large surface area and suitable pore size, as well as short diffusion distance of electrolyte ions in pore channels are desiderated for supercapacitor applications. Herein, we reported the synthesis of mesoporous activated carbon spheres (MACSs) that were obtained by the activation of resorcinol-formaldehyde (RF) resin using $ZnCl_2$ as the activating agent. The spherical morphology of MACSs was characterized by scanning electron microscopy and transmission electron microscopy observations, and the well-developed mesoporous network (~2.73 nm), high BET specific surface area (up to 2437.1 $m^2\ g^{-1}$), and total pore volume (1.37 $cm^3\ g^{-1}$) were obtained by a nitrogen sorption technique. Electrochemical measurements showed the excellent capacitive performance of MACSs and small internal resistance. It presented maximum specific capacitance value of 204 F g^{-1} for MACS-8 in 2 M KOH aqueous solution at a current density of 0.5 A g^{-1} and still remained 126 F g^{-1} at large current density as 20 A g^{-1}, which well met the practical requirements of supercapacitors. Besides, the electrode material also demonstrated prominent long-cycling stability without any capacity loss after 5000 cycles.

Keywords Activation · Porous carbon sphere · Zinc chloride · Resorcinol-formaldehyde resin · Supercapacitor

Electronic supplementary material The online version of this article (doi:10.1007/s10008-015-2789-8) contains supplementary material, which is available to authorized users.

Y. Wang · B. Chang · D. Guan · X. Dong (✉)
Department of Chemistry, School of Sciences, Zhejiang Sci-Tech University, 928 Second Avenue, Xiasha Higher Education Zone, Hangzhou 310018, China
e-mail: xpdong@zstu.edu.cn

Introduction

As high-rate energy storage and delivery devices, electrochemical supercapacitors have various potential applications in commercial fields such as consumer electronics, energy efficient industrial equipments, memory back-up systems and hybrid electric vehicles [1–3]. They are supposed to be promising alternatives of conventional batteries/capacitors for their outstanding advantages including high energy density and power density, fast charging-discharging rate, long cycle life, and low maintenance [4–7]. According to the energy-storage mechanism, supercapacitors can be classified into electrical double-layer capacitors (EDLCs) and pseudocapacitors. Taking advantage of their superior electronic conductivity and the absence of faradic reaction, EDLCs exhibit higher energy efficiency and longer recycle life in comparison with pseudocapacitors [8]. Up to date, EDLCs are dominant in commercial supercapacitors. The storage of electric energy in EDLCs is realized by the formation of electrical double layer at the interface between electrode materials and electrolyte [9]. Consequently, the surface properties of electrode materials including surface area and surface chemistry dramatically determine their energy-storing ability.

Porous carbons, such as activated carbons, regular microporous/ultramicroporous carbons, ordered mesoporous carbons, carbon nanotubes (CNTs), and graphene-based materials, are the most widely used electrode materials for EDLCs [10–17]. The capacitive performance of porous carbon materials strongly depends on their surface area and pore structure. Large surface area provides abundant regions for ion accumulation, thus enhances the electrochemical properties [18, 19]. Regardless of their large surface area, numerous irregular and island micropores in commercial activated carbon may limit the diffusion of electrolyte ions onto inner pore wall,

and large amounts of surface areas of micropores cannot participate in the charge-storage process of EDLCs, resulting in an unsatisfied capacitive performance of electrode materials [20]. Besides, macroporous structure facilitates the rapid transport of electrolyte ions in electrodes, whereas the surface area of electrode is severely limited in macroporous carbons. It has been demonstrated that mesoporous channels with pore size of 2–8 nm are not only favorable for accelerating the kinetic process of electrolyte ion diffusion in the electrodes, but also provide a quantity of inner surface area for storing charges, and subsequently improve the electrochemical performance [8, 21, 22]. Therefore, a variety of strategies, including template methods and chemical activation routes, have been developed for fabrication of carbonaceous materials with mesoporous structure [8, 16, 23, 24]. For example, Yuan et al. reported the highly ordered mesoporous carbon synthesized via hard template (silica) method with a specific capacitance of 161 F g^{-1} at the sweep rate of 5 mV s^{-1} [25]. Liang et al. reported the preparation of ordered mesoporous carbon by a soft template (triblock copolymer F127) method with a specific capacitance of 143 F g^{-1} at the scan rate of 10 mV s^{-1} [26]. Unfortunately, the high cost of templates, no matter mesoporous silica or copolymers, and the multistep process for synthesis of ordered mesoporous carbons limit their practical applications.

The mechanism of ion transport within porous channel system of electrode materials extremely relies on the pore structure including tortuosity, connectivity, size distribution, shape of the pores, as well as the nature of electrolyte ions and material interface [27–30]. Typically, small pore diameter restricts ion penetration within the pore channels, and the diffusion resistance increases dramatically with the decrease of pore size. The high ion transport resistance in inner pore may result in a serious internal resistance (IR) drop. Although mesopore size is well suited for the transport of electrolyte ions, the diffusion resistance of ions cannot be ignored especially charging at high charge-discharge rates. It has reported that long electrolyte diffusion distance always leads to a low ion-accessible surface area (S_{access}) at high current values, which has a bad effect on electrochemical properties [31]. Therefore, shortening ion diffusion distance in mesoporous channels is vital to improve capacitance performance of electrode materials, particularly when the current density is high. Obviously, mesoporous carbons with hierarchical structure such as macroporous/mesoporous structure and mesoporous carbons with nanoscale morphology (such as mesoporous fibrous materials, mesoporous carbon films) that effectively shorten the ion diffusion distance and accelerate the charge-discharge rates of EDLCs [32–34].

Mesoporous carbon nanospheres with regular geometry have been fabricated through different synthetic strategies using various precursors, such as resorcinol-formaldehyde resin [35, 36]. Herein, we addressed the design and preparation of mesoporous activated carbon spheres with superior porosity by a facile $ZnCl_2$ chemical activation method using RF resin with a nanospherical morphology as carbon source. The obtained MACS materials possess large surface area (2437.1 m^2 g^{-1}) and suitable pore size (~2.73 nm). And, the nanosized porous spherical structure can greatly shorten ion diffusion distance from bulk solution to active sites. When used as electrode materials for supercapacitors in 2 M KOH aqueous electrolyte, it exhibits more excellent capacitive properties than the comparative materials synthesized without $ZnCl_2$.

Experimental

All the chemical reagents in this work were of analytical grade purity and used without further purification.

Synthesis of RF resin nanospheres

Monodisperse RF resin spheres were synthesized by using resorcinol and formaldehyde solution, as previously reported [37]. Generally, 2.5-mL ammonia aqueous solution (NH_4OH, 25 wt%) was mixed with a solution containing 200 mL absolute ethanol and 500 mL deionized water (H_2O) and stirred for more than 1 h to form an aqueous ammonia-ethanol-water solvent. Five grams resorcinol was added to the mixed solution and stirred for 0.5 h. Then, 7-mL formaldehyde solution was added drop by drop and stirred for 24 h at 30 °C, and subsequently heated for 24 h at 100 °C under a static condition in an autoclave. The reddish-brown precipitate was collected by suction filtration and air-dried at 100 °C for 48 h.

Synthesis of MACSs by one-step $ZnCl_2$ activation of RF resin nanospheres

Typically, 40-mL $ZnCl_2$ aqueous solution was prepared, and 1-g RF resin was added into it. After stirring for 12 h under magnetic stirring apparatus, the mixture was air-dried at 110 °C overnight. The solid was ground into powder in the mortar and heated in a tube furnace under a nitrogen flow at 800 °C for 2 h with a heating rate of 2.5 °C/min. When cooling to room temperature, the as-prepared products were thoroughly washed with 1 M HCl and deionized water for several times then dried at 100 °C in oven. The resultant MACSs were denoted as MACS-x (x=4, 6, and 8, referring to the mass ratio of $ZnCl_2$/RF resin of 4:1, 6:1, and 8:1, respectively). For comparison, two control experiments were designed. The first comparative material was prepared by calcining RF resin at 800 °C without $ZnCl_2$, and the product was named as carbon sphere (CS). Second, RF resin was mixed with KOH at a KOH/RF resin mass ratio of 4:1 then treated under the same conditions. The obtained product was named as CS-KOH.

Characterization

Nitrogen adsorption-desorption isotherm measurements were carried out at −196 °C using a micromeritics ASAP 2020 surface area analyzer. Before adsorption, the samples were out-gassed at 150 °C for 6 h. The specific surface area (S_{BET}) was evaluated using the Brunauer-Emmett-Teller (BET) method, and the total pore volume was calculated according to single point method at relative pressure (P/P_0)= 0.975. The pore size distributions were estimated according to the density functional theory (DFT) method. Fourier transform infrared spectroscopy (FTIR) spectra of a sample in KBr pellet were recorded on a Nicolet Avatar 370 spectrometer. The morphology of the samples was observed by scanning electron microscope (SEM, Hitachi S-4800) and JEOL JEM-2100 transmission electron microscope (TEM) with an accelerating voltage of 200 KV.

Electrode preparation and electrochemical measurements

The electrochemical properties of MACSs and CS were evaluated at room temperature using an electrochemical workstation, CHI660B (Chenhua, Shanghai, China), with a three electrode system in a 2 M KOH aqueous solution. MACS served as the working electrode. Platinum was used as the counter electrode and Ag/AgCl as the reference electrode. The working electrode was fabricated as follows: 70 wt% active materials, 10 wt% acetylene black, and 20 wt% polyvinylidene fluoride (PVDF) were mixed together, and a small amount of absolute ethanol was added to promote homogeneity. Then, the slurry-like mixture was coated onto Ni foam (1 cm×1 cm) repeatedly and dried at 100 °C for 12 h before pressed under 20 MPa. The mass of active materials contained in each working electrode was about 5 mg. Cyclic voltammetry (CV) was performed under the voltage window from −1 to 0 V. The galvanostatic charge/discharge tests were carried out at current densities that ranged from 0.5 to 20 A g^{-1}. Electrochemical impedance spectroscopy (EIS) was measured at open circuit potential over a frequency range from 10 mHz to 100 kHz with an AC amplitude of 5 mV.

Results and discussion

Structure characteristics of MACSs

$ZnCl_2$ is often used to chemically activate carbonaceous materials to develop porous carbon with high surface area. $ZnCl_2$ acts as a dehydrating agent that stoichiometrically extracts those oxygen atoms and hydrogen atoms in organic groups by 1:2 as water molecules [38]. It promotes the decomposition of carbonaceous precursors during the high-temperature pyrolysis process, and products with higher carbon content were finally obtained. Meanwhile, vacant interstices in the carbon matrix are formed upon extensive postpyrolysis washing of the pores [39]. To study the reaction mechanism and the nanostructure of products, FTIR spectroscopy and nitrogen adsorption/desorption measurements are carried out.

FTIR spectroscopy (Fig. 1) is used to analyze the surface chemistry features of MACS, CS, and RF resin. Comparing with these curves of MACS and RF resin, it could be observed that large number of organic groups disappeared and nearly pure carbon was finally obtained by $ZnCl_2$ activation treatment. In the sample of RF resin, the absorption bands at 3430, 1630, and 1380–1480 cm^{-1} correspond to the stretching vibration of –OH from the surface of C–OH or water molecules, the skeleton vibration of aromatic C=C, and the C–H scissoring vibration, respectively [8]. The bands at 2850–2930 cm^{-1} are ascribed to the C–H symmetric stretching vibration and asymmetric stretching vibration [38]. Other bands at 1100–1250 cm^{-1} should be assigned to the C–O stretching vibration. For MACS, the bands of –OH and C=C are weakened significantly compared with RF resin which suggests the decrease of organic components in precursors. For comparison, it can be seen that there is still lots of C–H groups left in CS materials treated without $ZnCl_2$. A slightly red shift of the C=C absorption peak after calcination should be attributed to the reduction of $–CH_2–$ groups between aromatic rings that enhances the conjugative effect. Consequently, the absorption peaks of C–H and C–O disappeared during the high-temperature activation process, demonstrating that $ZnCl_2$ activation had a profound effect on the surface properties of MACS.

The amount of $ZnCl_2$ used for chemical activation controls the characteristics of porous carbons including surface area, microporosity and mesoporosity, and pore size distribution. In general, the chemical activation process of $ZnCl_2$ is divided into two steps that are described as the generation of microporous structure and the widening of pore size by the recombination of micropores. Generally speaking, the formation of micropores is predominant when the $ZnCl_2$/RF resin mass

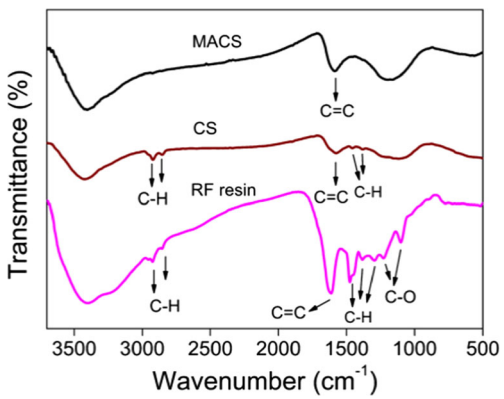

Fig. 1 FTIR spectra of MACS, CS, and resorcinol-formaldehyde resin

ratio is less than one, and the pore widening becomes dominant and mesopores are formed as the impregnation ratio is greater than 2 [39]. In consideration of the electrochemical application, an investigation with large mass ratios of $ZnCl_2$/RF resin was performed in this work for the purpose of preparing porous carbon materials with excellent mesoporous structure.

Nitrogen adsorption/desorption isotherms of MACSs and corresponding pore size distribution curves are shown in Fig. 2. MACS samples exhibit similar isotherms, and the adsorbed N_2 amount is rapidly enhanced from MACS-4 to MACS-6 and then slowly increases from MACS-6 to MACS-8. This result demonstrates that these MACS samples have similar porous structure and different surface areas and pore volumes. The isotherms of MACS samples display a rapid increment of N_2 adsorption from low pressure to medium pressure region, which can be attributed to a combined curve of type I and IV isotherms that indicates a transmitted porous structure from microporous to mesoporous. With a distinct contrast, the sample of CS without $ZnCl_2$ activation possesses a typical type I isotherm that is depicted in the inset of Fig. 2a and its sharp increase of adsorbed N_2 volume merely presents in the low pressure region, which is related to its microporous structure. The calculated pore size distribution (Fig. 2b) illustrates that MACSs possess similar pore structure with a distribution centered at ~2.73 nm and the pore size of CS is mainly distributed in micropore region.

The detail pore parameters including specific surface area, total pore volume (V_{total}), and pore diameter (D_p) are listed in Table 1. It can be observed that the pyrolysis of RF resin would produce certain porosity that results in BET surface area of 509.1 $m^2\ g^{-1}$ and pore volume of 0.26 $m^3\ g^{-1}$ in CS sample, which is mainly from its microporous structure. With addition of $ZnCl_2$ in the thermal treatment of RF resin, a significant enhancement of surface area and pore volume is achieved for MACSs, where the mesoporosity is dominant and total surface area and pore volume are from mesopores that proves the evolution of porous structure from microporous to mesoporous with the $ZnCl_2$ chemical activation. The increased trend of specific surface area and pore volume is in accordance with the adsorbed N_2 volume in Fig. 2a, and the

Table 1 Textural parameters of carbon materials derived from RF resin

Sample	S_{BET} [a] ($m^2\ g^{-1}$)	$S_{micropore}$ [b] ($m^2\ g^{-1}$)	$S_{mesopore}$ [c] ($m^2\ g^{-1}$)	V_{total} [d] ($cm^3\ g^{-1}$)	D_p [e] (nm)
MACS-4	1924.1	–	1976.5	1.11	2.73
MACS-6	2399.1	–	2498.0	1.35	2.73
MACS-8	2437.1	–	2615.0	1.37	2.73
CS	509.1	421.9	87.2	0.26	1.48/2.73

[a] Specific surface area estimated using BET method

[b] Micropore surface area calculated using the *V-t* plot method

[c] Mesopore surface area calculated using the *V-t* plot method

[d] Total pore volume using single point method at P/P_0=0.975

[e] Pore size calculated using DFT method

MACS-8 sample has a highest BET surface area of 2437.1 $m^2\ g^{-1}$ and a largest pore volume of 1.37 $cm^3\ g^{-1}$, which are higher than many other carbon-based materials (it can be seen in Table S1).

SEM and TEM measurements are taken to observe the nanostructure and morphology of the as-prepared electrode materials. From Fig. 3a, a monodisperse spherical shape with a diameter about 800 nm is found in RF resin. And, Fig. 3b shows a SEM image of MACS-8 with an average diameter of ~700 nm, which is smaller than that of RF resin due to the structure shrinkage in the thermal treatment. However, MACS-8 keeps an integrated spherical morphology with good dispersibility in solid phase. It reveals that the activation process by $ZnCl_2$ did not destroy the spherical morphology seriously. From the TEM images, there exist some flaws on the rough surface of mesoporous carbon that was partially etched due to $ZnCl_2$-activated behavior, which is responsible for the generation of mesopores. And, it can be found that the size of MACS-8 meets well with that in SEM and large amounts of nanopores on the sphere can be observed clearly. The activation process with dosage of $ZnCl_2$ can be studied from the TEM images of MACS-4, MACS-6, and MACS-8 (it can be seen in Fig. S1). This nanospherical morphology with well-developed porosity can reduce ion transport resistance and minimize ion diffusion distance to the interior surfaces of mesopores which enhances charge storage ability. The strong

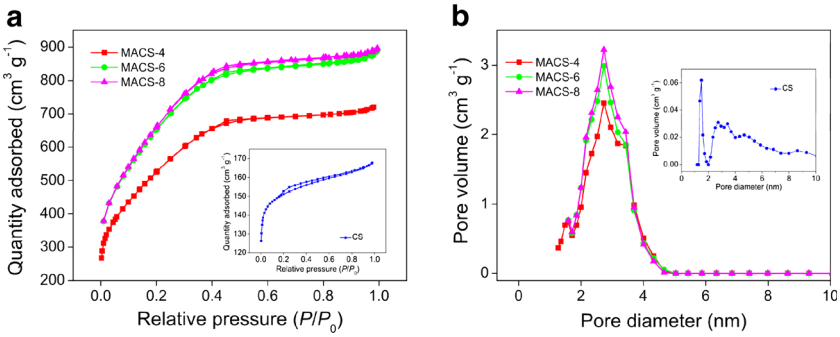

Fig. 2 **a** Nitrogen adsorption/desorption isotherms of MACSs (*inset* is the isotherm of CS); **b** the pore size distribution curves of MACSs (*inset* is the pore size distribution curve of CS)

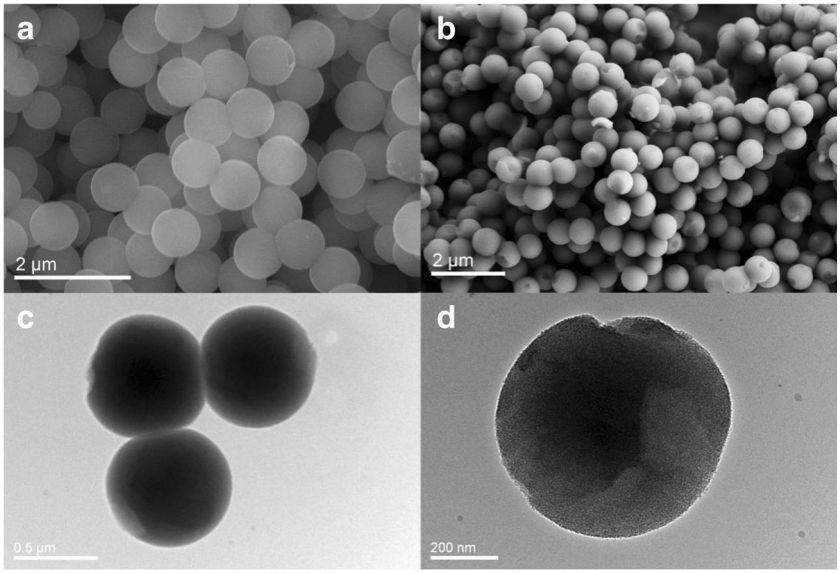

Fig. 3 SEM images of RF resin (**a**) and MACS-8 (**b**); TEM images of MACS-8 (**c**, **d**)

carbon framework makes it stable during fast charge-discharge process as well as long-time cycling.

Electrochemical performance of MACSs

Figure 4 compares the electrochemical performance of CS and MACSs prepared with various mass ratios of $ZnCl_2$/RF resin. As shown in Fig. 4a, CV curves of MACSs show similar rectangular shape but different areas that are proportional to the specific capacitance. The specific capacitance from CV curves at various scan rates were calculated by the following equation [40]:

$$C = \int I \mathrm{d}V \,/ mVv \tag{1}$$

where I (A) is the response current density, V (V) is the potential, v (mV s^{-1}) is the potential scan rate, and m (g) is the mass of electroactive material in the electrode. In comparison to the small rectangle of CS curve where the specific capacitance is calculated as 21.4 F g^{-1}, MACSs display relative large areas enclosed by their CV curves that increase with the enhancement of mass ratios of $ZnCl_2$/RF resin, and their corresponding specific capacitances are 124.6, 150.7, and 165.1 F g^{-1} with a scan rate of 50 mV s^{-1} for MACS-4, MACS-6, and MACS-8, respectively. Figure 4b shows the galvanostatic charge/discharge curves of these electrode materials at a constant current of 1 A g^{-1}. The galvanostatic discharge time of MACS-8 electrode is significantly longer than that of the control samples at the same current density, reflecting the higher specific capacitance, which is consistent with the CV results. The specific capacitances of MACSs based on galvanostatic charge/discharge curves were calculated according to the following formula [40]:

$$C = I\Delta t / m\Delta V \tag{2}$$

where I (A) is the discharging current, Δt (s) is the discharging time, m (g) is the mass of electrode material, ΔV (V) is the discharging potential range, and C (F g^{-1}) is the specific capacitance of the electrode. The specific capacitances are calculated from the discharge curves with values of 196.2, 182.2, and 157.4 F g^{-1} at a constant current of 1 A g^{-1} for MACS-8, MACS-6, and MACS-4, respectively. It is clear that MACS-8

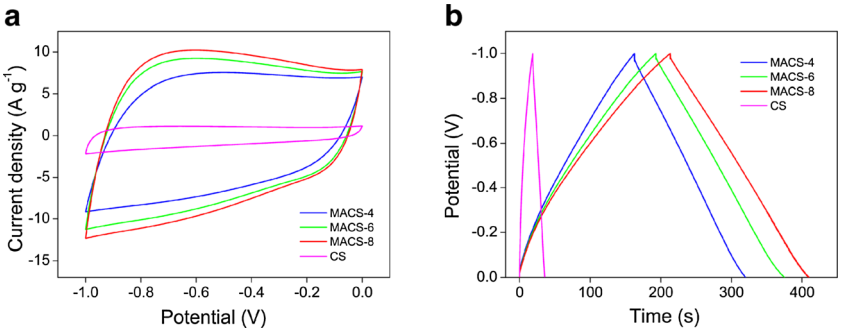

Fig. 4 Comparison of electrochemical properties between MACSs and CS: **a** cyclic voltammograms at the sweep rate of 50 mV s^{-1}; **b** galvanostatic charge/discharge curves at the current density of 1 A g^{-1}

presents the best capacitance performance among these materials. CS activated without $ZnCl_2$ shows a short discharging time, and the capacitance decreases sharply to 16.9 F g^{-1}, which is much lower than MACSs. This should be ascribed to its large amount of microporous textures and low specific area. Meanwhile, as is typically observed for EDLCs, the initial portion of discharge curves exhibit a slight IR drop due to the internal resistance and the rest are almost linear. As an outstanding activating agent, KOH has been widely used to prepare porous carbon electrode materials. Figure S2 shows that CS-KOH possess superior capacity performance with specific capacitance of 171.6 F g^{-1} at 50 mV s^{-1} and 198.1 F g^{-1} at 1 A g^{-1} which is comparable with our sample. But, the low yield and other limits of KOH-activated method cannot be ignored. In our work, the yield of CS-KOH (~16 %) is much lower than MACS-8 (~53 %) due to different activation mechanisms. High yield is of great important to practical application, and $ZnCl_2$-activation method is able to meet this demand very well.

Electrochemical behaviors of the optimal sample of MACS-8 were further investigated, including CV curves with various scan rates, galvanostatic charge/discharge against current densities, long-cycle stability, and electrochemical impedance spectroscopy. Figure 5a shows typical CV curves with a nearly rectangular shape with no obvious redox peaks that suggests the characteristics of EDLCs and the stability of electrodes in alkaline electrolyte solution. As the scan rate increases, the symmetrical rectangular shape becomes distorted due to the IR increase of electrode and electrolyte [4]. It is well known that the specific capacitance of activated carbon materials is 10–15 μF cm^{-2} [41]; thus, MACS-8 (S_{BET}=2437.1 m^2 g^{-1}) should possess a theoretical capacitance value of 244–366 F g^{-1}. The calculated specific capacitance from CV is 210 F g^{-1} at the scan rate of 2 mV s^{-1}, suggesting the excellent capacity performance (about 57.4–86.1 % of theoretical value). Galvanostatic charge/discharge measurements at current densities ranging from 0.5 to 20 A g^{-1} were performed, and the results are shown in Fig. 5b. It exhibits highly symmetric charging/discharging curves with isosceles triangular shapes, indicating an almost ideal EDLC behavior and reversibility of the capacitance. The calculated specific capacitance value of MACS-8 reaches 204 F g^{-1} at current density of 0.5 A g^{-1} that is much higher than those of other porous carbon materials synthesized by different methods (Table S1). This excellent capacitive behavior should be attributed to the superior mesoporosity and high surface area, as well as the nanospherical morphology. A small voltage drop observed at the initiation of the discharge is 0.024 V (for the current density of 1 A g^{-1}), suggesting that these materials possess an excellent rate performance [11]. The relationship between specific capacitance and current densities is shown in Fig. 5c, which shows that the specific capacitance value progressively decreases as the current density increases because of the limitation of ion diffusion in pore channels. Nonetheless, a good retention of specific capacitance as high as 126 F g^{-1} is achieved at current density up to 20 A g^{-1}. This suggests that MACS-8 sample possesses an excellent charging-discharging ability under both small and large current densities that well meets the high-power operation demand for EDLCs.

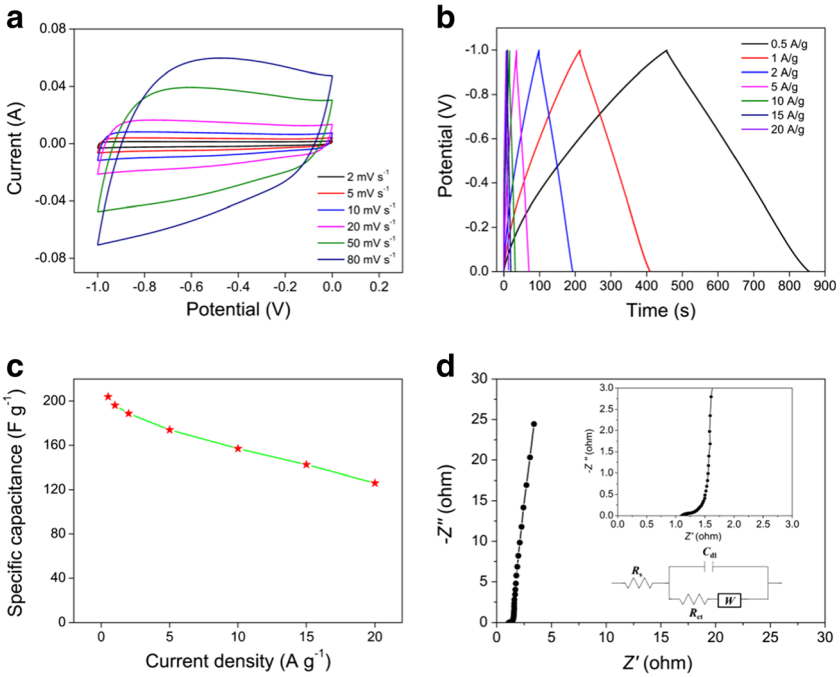

Fig. 5 Electrochemical performance of the MACS-8 measured in 2 M KOH aqueous solution: **a** cyclic voltammograms at different scan rates; **b** galvanostatic charge/discharge curves at current densities in the range of 0.5 to 20 A g^{-1}; **c** the relationship between specific capacitance and several current densities; **d** electrochemical impedance spectroscopy of MACS-8 (*inset* is the magnified view of Nyquist plots and the equivalent circuit)

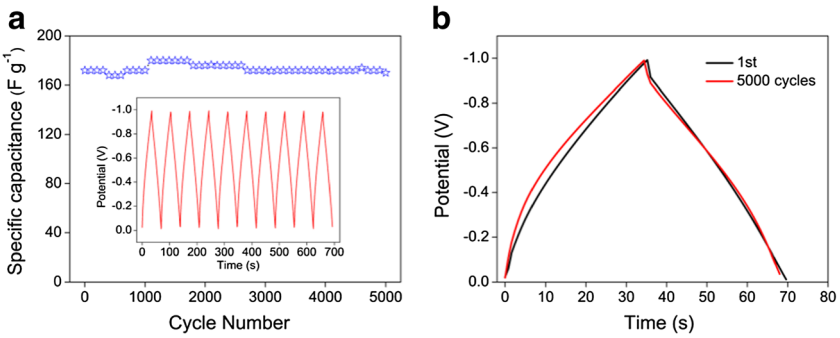

Fig. 6 **a** Specific capacitance versus cycling number at 5 A g^{-1} for 5000 cycles (the *inset* shows the first 10 charge-discharge cycle curves of the test). **b** Comparison of charge-discharge curve for the first cycle and 5000_{th} cycle

Electrochemical impedance spectroscopy (EIS) is a powerful technique to investigate the electrochemical behaviors of the electrode materials. A small semicircle in high-frequency region is related to the interfacial charge-transfer process, and the diameter of semicircle corresponds to the charge-transfer resistance (R_{ct}). The 45° segment in the Nyquist plot in high-frequency region represents a Warburg impedance (W) that describes the diffusion resistance of ions in electrolyte to porous structure. The steep line with high slope in low-frequency region indicates the nearly ideal capacitive behavior, which is related to electrolyte diffusion and migration within the porous electrode networks [8]. Besides, the intercept of the EIS curve at Z' axis corresponds to the solution resistance (R_s) and it mainly depends on the resistance of the electrolyte, the intrinsic resistance of active materials, and the contact resistance between active materials and nickel foam current collector. The inset of Fig. 5d shows the equivalent circuit which is consisted of R_s, R_{ct}, a double-layer capacitance C_{dl} and the Warburg impedance W. The R_{ct} and R_s values calculated from impedance data are 0.23 Ω and 1.1 Ω, respectively, referring low charge-transfer and internal resistance of the MACS-8 electrode. The low resistance of as-prepared materials may result from high crystalline degree that greatly enhances the good conductivity of MACS-8 electrodes. The specific capacitance from impedance spectroscopy can be calculated using the following formula [42]:

$$C = -1/2\pi f Z'' \tag{3}$$

where C is the capacitance (frequency dependent), f is the frequency, and Z'' is the imaginary part of the impedance. The specific capacitance value for MACS-8 electrode is 169 F g^{-1} at 0.01 Hz, which is in conformity with that measured by cyclic voltammetric and galvanostatic charge-discharge methods.

Another crucial demand for supercapacitor application is the long-cycling stability. It was measured by means of galvanostatic charge-discharge cycling techniques at the current density of 5 A g^{-1} in 2 M KOH solution. As can be seen from Fig. 6a, the electrochemical capacitance of MACS-8 electrode has a high retention of 100 % after 5000 constant current cycles, meaning the good charge/discharge stability as electrode materials of EDLCs. It should be assigned to the stable microstructure despite of ion transport and charge transfer. The capacitance fluctuation at first 1000 cycles may arise from contact effect between electrode materials and electrolyte. Moreover, the specific capacitance increases during 1000–2000 cycles, and it may be ascribed to faster diffusing rate of electrolyte ions to the surface of MACS-8 caused by the long-term penetration of electrolyte. The inset shows the first 10 cycles obtained from the long cycling tests. Figure 6b shows the charge-discharge curves of the first and the 5000_{th} cycle. It can be seen that the charge-discharge curves retained the similar triangular shape with almost same discharge time. This is in accordance with the result of Fig. 6a. However, the IR drop increases from 0.084 to 0.11 V, suggesting a small increase of internal resistance for MACS-8 electrode after 5000 cycles.

Conclusion

In this study, an easy procedure was proposed for synthesis of mesoporous activated carbon spheres derived from RF resin by high-temperature activation with $ZnCl_2$. The chemical activation method dramatically enhances the surface area and the generation of mesopores. The prepared materials show extremely large surface area, large pore volume, and outstanding mesoporous structure. Benefiting from the various advantages, MACSs exhibit excellent electrochemical performances for EDLCs such as high specific capacitance and low internal resistance. They also present excellent electrochemical behavior at high charge-discharge current. The long-term cycling stability is also superior for our electrodes, and there is almost no capacity loss after 5000 charge-discharge cycles. This easy and low-cost method supplies an alternative route to synthesize electrode materials for electrochemical energy storage devices.

Acknowledgments The authors gratefully acknowledge the financial support from 521 talent project of ZSTU, the program of Graduate Innovation Research in ZSTU (YCX13001), and the project-sponsored by the Scientific Research Foundation (SRF) for the Returned Overseas Chinese Scholars (ROCS), State Education Ministry (SEM).

References

1. Kim TY, Jung G, Yoo S, Suh KS, Ruoff RS (2013) Activated graphene-based carbons as supercapacitor electrodes with macro- and mesopores. ACS Nano 7:6899–6905
2. Wei L, Sevilla M, Fuertes AB, Mokaya R, Yushin G (2012) Polypyrrole-derived activated carbons for high-performance electrical double-layer capacitors with ionic liquid electrolyte. Adv Funct Mater 22:827–834
3. Wang Y, Shi Z, Huang Y, Ma Y, Wang C, Chen M, Chen Y (2009) Supercapacitor devices based on graphene materials. J Phys Chem C 113:13103–13107
4. Zhang J, Lee JW (2014) Supercapacitor electrodes derived from carbon dioxide. ACS Sustain Chem Eng 2:735–740
5. Ruiz V, Pandolfo AG (2011) High-frequency carbon supercapacitors from polyfurfuryl alcohol. J Power Sources 196:7816–7822
6. Liu C, Yu Z, Neff D, Zhamu A, Jang BZ (2010) Graphene-based supercapacitor with an ultrahigh energy density. Nano Lett 10:4863–4868
7. Zhou X, Li L, Dong S, Chen X, Han P, Xu H, Yao J, Shang C, Liu Z, Cui G (2012) A renewable bamboo carbon/polyaniline composite for a high-performance supercapacitor electrode material. J Solid State Electrochem 16:877–882
8. Li M, Liu C, Cao H, Zhao H, Zhang Y, Fan Z (2014) KOH self-templating synthesis of three-dimensional hierarchical porous carbon materials for high performance supercapacitors. J Mater Chem Res A 2:14844–14851
9. Zhu Y, Murali S, Stoller MD, Ganesh KJ, Cai W, Ferreira PJ, Pirkle A, Wallace RM, Cychosz KA, Thommes M, Su D, Stach EA, Ruoff RS (2011) Carbon-based supercapacitors produced by activation of graphene. Science 332:1537–1541
10. Tan Y, Xu C, Chen G, Liu Z, Ma M, Xie Q, Zheng N, Yao S (2013) Synthesis of ultrathin nitrogen-doped graphitic carbon nanocages as advanced electrode materials for supercapacitor. ACS Appl Mater Interfaces 5:2241–2248
11. Sevilla M, Fuertes AB (2014) Direct synthesis of highly porous interconnected carbon nanosheets and their application as high-performance supercapacitors. ACS Nano 8:5069–5078
12. Wahid M, Puthusseri D, Phase D, Ogale S (2014) Enhanced capacitance retention in a supercapacitor made of carbon from sugarcane bagasse by hydrothermal pretreatment. Energy Fuels 28:4233–4240
13. Mishra AK, Ramaprabhu S (2011) Functionalized graphene-based nanocomposites for supercapacitor application. J Phys Chem C 115:14006–14013
14. Jin YZ, Kim YJ, Gao C, Zhu YQ, Huczko A, Endo M, Kroto HW (2006) High temperature annealing effects on carbon spheres and their applications as anode materials in Li-ion secondary battery. Carbon 44:724–729
15. Lin JH, Ko TH, Lin YH, Pan CK (2009) Various treated conditions to prepare porous activated carbon fiber for application in supercapacitor electrodes. Energy Fuels 23:4668–4677
16. Zhao Y, Liu M, Gan L, Ma X, Zhu D, Xu Z, Chen L (2014) Ultramicroporous carbon nanoparticles for the high-performance electrical double-layer capacitor electrode. Energy Fuels 28:1561–1568
17. Zhao Y, Liu M, Deng X, Miao L, Tripathi PK, Ma X, Zhu D, Xu Z, Hao Z, Gan L (2015) Nitrogen-functionalized microporous carbon nanoparticles for high performance supercapacitor electrode. Electrochim Acta 153:448–455
18. Wang K, Wang Y, Wang Y, Hosono E, Zhou H (2009) Mesoporous carbon nanofibers for supercapacitor application. J Phys Chem C 113:1093–1097
19. Li W, Zhang F, Dou Y, Wu Z, Liu H, Qian X, Gu D, Xia Y, Tu B, Zhao D (2011) A self-template strategy for the synthesis of mesoporous carbon nanofibers as advanced supercapacitor electrodes. Adv Energy Mater 1:382–386
20. Pol VG, Shrestha LK, Ariga K (2014) Tunable, functional carbon spheres derived from rapid synthesis of resorcinol-formaldehyde resins. ACS Appl Mater Interfaces 6:10649–10655
21. Ma X, Liu M, Gan L, Zhao Y, Chen L (2013) Synthesis of micro- and mesoporous carbon spheres for supercapacitor electrode. J Solid State Electrochem 17:2293–2301
22. Zhang LL, Zhao XS (2009) Carbon-based materials as supercapacitor electrodes. Chem Soc Rev 38:2520–2531
23. Yin H, Lu B, Xu Y, Tang D, Mao X, Xiao W, Wang D, Alshawabkeh AN (2014) Harvesting capacitive carbon by carbonization of waste biomass in molten salts. Environ Sci Technol 48:8101–8108
24. Zhai D, Du H, Li B, Zhu Y, Kang F (2011) Porous graphitic carbons prepared by combining chemical activation with catalytic graphitization. Carbon 49:725–736
25. Yuan DS, Zeng J, Chen J, Liu Y (2009) Highly ordered mesoporous carbon synthesized via in situ template for supercapacitors. Int J Electrochem Sci 4:562–570
26. Liang Y, Wu D, Fu R (2009) Preparation and electrochemical performance of novel ordered mesoporous carbon with an interconnected channel structure. Langmuir 25:7783–7785
27. Wen ZB, Qu QT, Gao Q, Zheng XW, Hu ZH, Wu YP, Liu YF, Wang XJ (2009) An activated carbon with high capacitance from carbonization of a resorcinol-formaldehyde resin. Electrochem Commun 11:715–718
28. Yamada H, Nakamura H, Nakahara F, Moriguchi I, Kudo T (2007) Electrochemical study of high electrochemical double layer capacitance of ordered porous carbons with both meso/macropores and micropores. J Phys Chem C 111:227–233
29. Dai Y, Jiang H, Hu Y, Fu Y, Li C (2014) Controlled synthesis of ultrathin hollow mesoporous carbon nanospheres for supercapacitor applications. Ind Eng Chem Res 53:3125–3130
30. Hao L, Li X, Zhi L (2013) Carbonaceous electrode materials for supercapacitors. Adv Mater 25:3899–3904
31. Wang DW, Li F, Liu M, Lu GQ, Cheng HM (2008) 3D aperiodic hierarchical porous graphitic carbon materials for high-rate electrochemical capacitive energy storage. Angew Chem Int Ed 47:373–376
32. Feng D, Lv Y, Wu Z, Dou Y, Han L, Sun Z, Xia Y, Zheng G, Zhao D (2011) Free-standing mesoporous carbon thin films with highly ordered pore architectures for nanodevices. J Am Chem Soc 133:15148–15156
33. Le VT, Kim H, Ghosh A, Kim J, Chang J, Vu QA, Pham DT, Lee JH, Kim SW, Lee YH (2013) Coaxial fiber supercapacitor using all-carbon material electrodes. ACS Nano 7:5940–5947
34. Yue Z, Mangun CL, Economy J (2002) Preparation of fibrous porous materials by chemical activation: 1. $ZnCl_2$ activation of polymer-coated fibers. Carbon 40:1181–1191
35. Ma X, Gan L, Liu M, Tripathi PK, Zhao Y, Xu Z, Zhu D, Chen L (2014) Mesoporous size controllable carbon microspheres and their electrochemical performance for supercapacitor electrodes. J Mater Chem A 2:8407–8415
36. Xiong W, Liu M, Gan L, Lv Y, Li Y, Yang L, Xu Z, Hao Z, Liu H, Chen L (2011) A novel synthesis of mesoporous carbon microspheres for supercapacitor electrodes. J Power Sources 196:10461–10464
37. Liu J, Qiao SZ, Liu H, Chen J, Orpe A, Zhao D, Lu GQ (2011) Extension of the stöber method to the preparation of monodisperse

resorcinol-formaldehyde resin polymer and carbon spheres. Angew Chem Int Ed 50:5947–5951
38. Chang B, Guan D, Tian Y, Yang Z, Dong X (2013) Convenient synthesis of porous carbon nanospheres with tunable pore structure and excellent adsorption capacity. J Hazard Mater 262:256–264
39. Khalili NR, Campbell M, Sandi G, Golas J (2000) Production of micro- and mesoporous activated carbon from paper mill sludge I. effect of zinc chloride activation. Carbon 38:1905–1915
40. Chang B, Wang Y, Pei K, Yang S, Dong X (2014) $ZnCl_2$-activated porous carbon spheres with high surface area and superior mesoporous structure as an efficient supercapacitor electrode. RSC Adv 4: 40546–40552
41. Zhao X, Tian H, Zhu M, Tian K, Wang JJ, Kang F, Outlaw RA (2009) Carbon nanosheets as the electrode material in supercapacitors. J Power Sources 194:1208–1212
42. Li L, Song H, Chen X (2006) Pore characteristics and electrochemical performance of ordered mesoporous carbons for electric double-layer capacitors. Electrochim Acta 51:5715–5720
43. Kim C, Ngoc BTN, Yang KS, Kojima M, Kim YA, Kim YJ, Endo M, Yang SC (2007) Self-sustained thin webs consisting of porous carbon nanofibers for supercapacitors via the electrospinning of polyacrylonitrile solutions containing zinc chloride. Adv Mater 19:2341–2346
44. He X, Li R, Han J, Yu M, Wu M (2013) Facile preparation of mesoporous carbons for supercapacitors by one-step microwave-assisted $ZnCl_2$ activation. Mater Lett 94:158–160